Journal of Molecular Liquids 342 (2021) 117478

Contents lists available at ScienceDirect

Journal of Molecular Liquids

journal homepage: www.elsevier.com/locate/molliq

Comparison of atomic simulation methods for computing thermal conductivity of *n*-decane at sub/supercritical pressure

Xueming Yang [a,*], Yue Gao [a], Mingli Zhang [a], Wenchao Jiang [a], Bingyang Cao [b,*]

[a] Hebei Key Laboratory of Low Carbon and High Efficiency Power Generation Technology, Department of Power Engineering, North China Electric Power University, Baoding 071003, China

[b] Key Laboratory for Thermal Science and Power Engineering of Ministry of Education, Department of Engineering Mechanics, Tsinghua University, Beijing 100084, China

ARTICLE INFO

Article history:
Received 16 June 2021
Revised 1 September 2021
Accepted 3 September 2021
Available online 8 September 2021

Keywords:
RP-3 aviation kerosene
Thermal conductivity
N-alkanes
Molecular dynamic

ABSTRACT

n-Decane is the most commonly used component in surrogate to study the properties of RP-3 aviation kerosene for regenerative cooling systems and the engine injection systems. In this paper, the equilibrium molecular dynamics (EMD) and the reverse non-equilibrium MD (RNEMD) methods are adopted and compared in the prediction of the thermal conductivity of the sub/supercritical *n*-decane. Four different united atom (UA) force field models and four all-atomic force field models are compared in the EMD simulations. It is found that the UA models predict much better than the all-atom force field models and EMD methods show better prediction accuracy than the RNEMD methods with the same UA models. The SKS model has the best prediction accuracy among all the force field models for EMD and RNEMD simulations. The MD results are compared with experimental data of RP-3 aviation kerosene; it is obtained that the overall averaged absolute relative deviation (AARD) of EMD simulations with the SKS force field model for the single component substitute of aviation kerosene by *n*-decane is 2.05%. Moreover, the radial distribution functions are calculated via MD simulations to make a better understanding of the temperature dependences of the thermal conductivity at sub/supercritical pressure of *n*-decane at a molecular level. The findings of this work could provide important guidance for the investigation of thermal conductivity of n-alkanes and n-alkane-based fuels.

1. Introduction

With the development of scramjets, more attention has been paid to the physical parameter analysis, flow heat transfer and thermal cracking of hydrocarbon fuel in the regenerative cooling channel of aero engine cooling systems [1–4]. Aviation fuel has been used as a cold source to reduce the temperature of the turbine cooling air through a heat exchanger. As a typical aviation fuel, aviation kerosene has gained more research interest for its heat transfer characteristics under supercritical pressure. However, aviation kerosene is made up of hundreds of hydrocarbons with complex components, including paraffins, cycloalkanes, olefins, and aromatic hydrocarbons, and it is impossible to study and analyze the entire components. In practical studies, the "alternative fuel" method based on the mixture of several typical basic components to represent the physical and chemical properties of real fuels has been proposed and widely used [5–7].

Many theoretical studies have been made on the surrogate single- or multi-component blend of pure hydrocarbons for alternatively describing the complex aviation fuels. By using a kinetic model, Violi et al. [8] proposed the 6-component alternative fuel for French aviation kerosene JP-8 and discussed the chemical dynamics model of jet fuel. Dagaut [9] utilized a kinetic model to investigate the reaction mechanisms and found a 3-component alternative fuel model for JP-8. Huber et al. [10] mathematically built a mixture model explicit in the Helmholtz energy and proposed a 7-component alternative model to simulate the thermophysical properties of aviation fuel S-8. Liu et al. [11] studied the *n*-decane chemical reaction mechanism using pre-evaporation combustion models, and found that *n*-decane can be used as a one-component surrogate fuel for RP-3 aviation kerosene to model the combustion characteristics. Yan et al. [12] presented a two-component surrogate fuel model with 92% *n*-decane and 8% n-propyl benzene for combustion of RP-3 kerosene surrogate fuel using the direct relation graph method. Liu et al. [13] formulated a 5-component surrogate fuel by an optimization algorithm to reproduce the ignition and laminar combustion properties of RP-3 kerosene. Based on the extended law of corresponding states,

* Corresponding authors.
E-mail addresses: xuemingyang@ncepu.edu.cn (X. Yang), caoby@tsinghua.edu.cn (B. Cao).

https://doi.org/10.1016/j.molliq.2021.117478
0167-7322/

Xu et al. [14] calculated the thermophysical properties of aviation kerosene RP-3 and found that simple surrogate models containing the *n*-decane species can provide reasonable accuracy. For RP-3 kerosene, *n*-decane is the most commonly used surrogate component in the study of its thermophysical and chemical properties. The critical pressure of *n*-decane is 2.103 MPa and the critical temperature is 617.7 K [15].

Molecular dynamics (MD) simulations provide an alternative way to study the thermophysical properties of alkanes [16,17]. In recent years, MD simulations have become important in studying the transport properties of working fluids [18–20]. Thermal conductivity is an important thermodynamic parameter in the thermal management system design, and accurate prediction and analysis of the thermal conductivity of the aviation fuel are required. For thermal conductivities of *n*-decane, some experimental works [21,22] have been reported, however the experimental data is limited and studies carried out above 390 K is very few [23]. Although many MD studies have been conducted on the thermophysical properties of alkanes, such as density, shear viscosity, and self-diffusion coefficient, however, MD studies of the thermal conductivity of alkanes are rare [24]. To the best of the authors' knowledge, no MD study on thermal conductivities of *n*-decane was conducted at sub/supercritical pressure. Moreover, the prediction accuracy of MD simulations depend not only the methods but also the force field models adopted; thus a comparison of MD methods and the different force field models for the prediction of the thermal conductivity of alkanes is necessary.

In this study, equilibrium molecular dynamics (EMD) method and the reverse non-equilibrium MD (RNEMD) method are adopted and compared in the prediction of the thermal conductivity of the sub/supercritical *n*-decane. Four different united atom (UA) force field models and four all-atomic field models are compared in the EMD simulations. One-component surrogate by *n*-decane for RP-3 aviation kerosene is also discussed. The numerical data and uncertainty estimates are provided in the supplementary material to allow readers to compare the obtained calculations.

2. Models and methodology

2.1. Force field models

Four united atom force field (UA) models are adopted and compared in our MD simulations, including SKS [25,26], TraPPE-UA [27], NERD [28], and OPLS-UA [29]. In the UA models, each CH_2 and CH_3 is represented by a pseudoatom, which is combined with other pseudoatoms to represent linear chain molecules [19], as shown in Fig. 1.

The unit sizes of CH_3 and CH_2 are expressed by σ_{CH_3} and σ_{CH_2} respectively, and the action sites of force field parameters of different elements are determined by the standard Lorentz-Berthelot.

$$\varepsilon_{ij} = (\varepsilon_{ii}\varepsilon_{jj})^{1/2} \text{ and } \sigma_{ij} = \frac{\sigma_{ii} + \sigma_{jj}}{2} \tag{1}$$

n-Decane molecules are nonpolar under these simulation conditions, and the long-range electrostatic forces and Coulomb forces are ignored. The energy system is calculated using the above four model force fields as shown in the following formula.

$$V = V(r)/k_B + V(\theta)/k_B + V(\phi)/k_B + V(r_{ij}) \tag{2}$$

where $V(r)$,$V(\theta)$, $V(\phi)$ and $V(r_{ij})$ represent contributions of bond stretching, angle bending, torsion angle and van der Waals interactions [27], respectively. The Lennard-Jones(12–6) potentials are used to describe the van der Waals interaction. Each term of Eq. (2) can be expressed as follows:

$$V(r)/k_B = \frac{K_r}{2}(r - b_{eq})^2 \tag{3}$$

$$V(\theta)/k_B = \frac{K_\theta}{2}(\theta - \theta_{eq})^2 \tag{4}$$

$$V(\phi)/k_B = V_0 + V_1(1 + \cos\phi) + V_2(1 - \cos 2\phi) + V_3(1 + \cos 3\phi) \tag{5}$$

$$V(r_{ij}) = 4\varepsilon_{ij}\left[\left(\frac{\sigma_{ij}}{r_{ij}}\right)^{12} - \left(\frac{\sigma_{ij}}{r_{ij}}\right)^{6}\right] \tag{6}$$

where b_{eq}, θ_{eq} and ϕ denote equilibrium lengths of bond, equilibrium values of angle, and dihedral angles, respectively. $V_i\{i = 0, 1, 2, 3\}$ are forcefield-specific coefficients. The non-bonded interactions are described by the last two terms, in which r_{ij} denotes the inter-atom distance, and σ_{ij} and ε_{ij} denote the interaction parameters of L-J potential which represent the energy parameter and scale parameter, respectively. The united force field parameters for the *n*-decane models are shown in Table 1.

In addition, four all-atom force field are also adopted for comparison with the UA models in our MD simulations, including COMPASS [30], OPLS-AA [31], AMBER [32], and L-OPLS [33], the details of the parameters of these models can be found in Refs. [30–33].

2.2. EMD and RNEMD method

For EMD simulation with the Green-Kubo method, the thermal conductivity can be calculated as the integral of the heat flow autocorrelation function [34], as follows:

$$\lambda = \frac{1}{3k_B V T^2}\int_0^\infty \left\langle \vec{J}(0)\cdot\vec{J}(t)\right\rangle dt \tag{7}$$

where V is the volume of the system, k_B is Boltzmann constant, and T is the temperature of the system. $\vec{J}$ represents the heat current at time t, $\left\langle \vec{J}(0)\cdot\vec{J}(t)\right\rangle$ denotes the heat current autocorrelation function (HCACF), where $\vec{J}(t) = \sum_i \vec{v}_i\vec{\varepsilon}_i + \frac{1}{2}\sum_{i,j,i\neq j}\vec{r}_{ij}(\vec{F}_{ij}\cdot\vec{v}_{ij})$. $\vec{\varepsilon}_i$ is the total energy including kinetic energy and potential energy, and it can be expressed as $\vec{\varepsilon}_i = \frac{1}{2}m_i\vec{v}_i + \frac{1}{2}\sum_{j\neq i}\varphi(\vec{r}_{ij})$, where $\varphi(\vec{r}_{ij})$ denotes the energy between two adjacent atoms. $\vec{v}_i$,$\vec{r}_{ij}$ respectively represent the kinetic energy of ith atom and the distance between atoms at different positions.

The RNEMD method proposed by Muller-Plathe [35] which can be applied to calculate thermal conductivity according to the Fourier law as follows:

$$\lambda = -\frac{J_Z}{dT/dz} \tag{8}$$

where J_Z, dT/dzrespectively represents the heat flux in the z direction and the temperature gradient obtained along the z direction.

2.3. Simulation details

All MD simulations are performed using the Large-scale Atomic/Molecular Massively Parallel Simulator (LAMMPS) package [36]. The EMD simulations are carried out in 3D cubic box with periodic boundary conditions applied along the x-, y- and z-directions to avoid edge effects on the bulk fluid [25]. The time step is set as 1 fs. The cut-off distance for L-J interactions are chosen as $r_c = 3.5\sigma$[28]. For the simulations with all-atom models, columbic interactions for a distance of two atoms shorter than 1.8 nm are calculated directly [37], while those further are calculated through

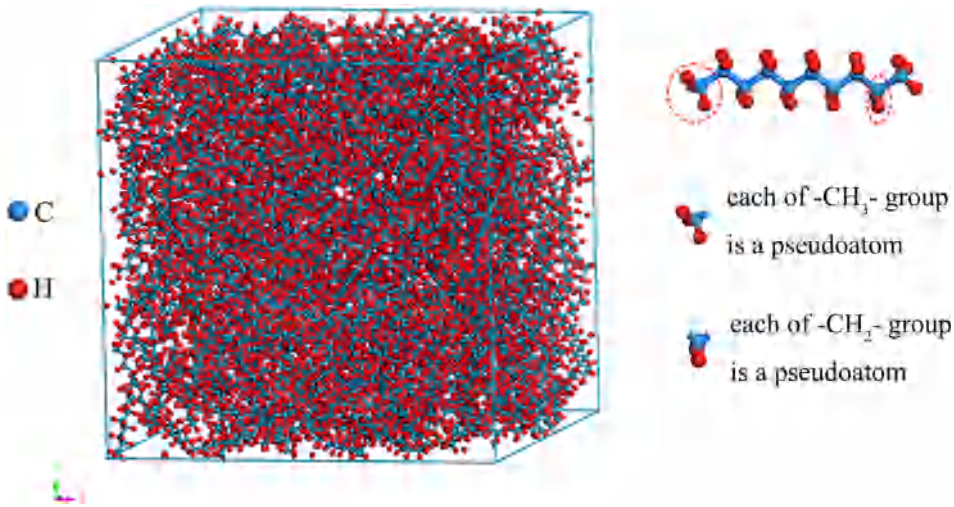

Fig. 1. (color online). Simulation system for the calculation of thermal conductivity of *n*-decane via UA models.

the particle–particle/particle-mesh (PPPM) method [38] with a precision of 10^{-5} [39]. The minimization of energy is carried out through the steepest descent method [37]. The simulations initially run for 500 ps in an isochoric-isothermal (NVT) ensemble to control the system temperature. Then it is switched to the isobaric-isothermal (NPT) and equilibrate the system at a given pressure and temperature for 500 ps. Finally, the micro-canonical ensemble (NVE) is used and simulations run for 500 ps for relaxation, and the following 2.5 ns is used for production and output. In the RNEMD simulations, the simulation box filled with 500 *n*-decane molecules of size 3L × 3L × 20L(3L = 29 Å) is used [24]. Simulations details including the boundary conditions, time step, r_c, and ensembles are the same as those which have been used during EMD simulations, except an final 5 ns is used to generate outputs.

3. Results and discussion

3.1. Prediction results by EMD simulations

The strategies of EMD simulations are adopted similar to those in our previous studies [40–42]. To overcome the uncertainties of the results associated with the EMD simulations, the thermal conductivity is averaged over six independent runs where initial velocity has been changed prior to each run. In earlier studies [40,43] for transport properties of fluids, it has been found that five or more independent simulations are enough and can ensures a good balance of accuracy and efficiency for the simulations. To select the appropriate correlation time [44], the normalized HCACF of *n*-decane is calculated. Fig. 2(a) shows the normalized HCACF in six independent runs of EMD simulations with the SKS model, in which the red line represents the averaged normalized HCACF of the six independent runs, while other lines represent the normalized HCACF results in each individual run. In Fig. 2(b), the averaged normalized HCACF of EMD simulations with four different UA models are compared. It can be observed that the normalized HCACF decays to zero at around 7500 fs for EMD simulations with different UA models. Therefore we select a correlation time of 7500 fs in the EMD simulations of the thermal conductivity.

In Fig. 3(a), the red line represents the averaged thermal conductivity of the six independent runs, while other lines represent the thermal conductivity results for each individual run. Fig. 3(b) represents the averaged thermal conductivity of EMD simulations with different UA models. To test the influence of the system size on simulation, series EMD simulations are conducted with different system sizes (*n*-decane molecules are taken as N = 125, 250, 500 and 1000) at a pressure of 3 MPa and temperature of 298.87 K. The calculated thermal conductivities are compared with the reference data from National Institute of Standards and Technology (NIST) [42], as shown in Fig. 4. It can be observed that the calculated thermal conductivity is in good agreement with NIST data and not sensitive to the system size.

Since the prediction accuracy of the MD simulations method largely depend on the force field model adopted, evaluation of the prediction accuracy of different force field models is necessary. To clarify the discussion, the absolute relative deviation (ARD)

Table 1
Parametric model of the united atom force fields.

Model		SKS [25,26]	TraPPE-UA [27]	NERD [28]	OPLS-UA [29]
σ_{CH_3}	(Å)	3.93	3.77	3.91	3.905
σ_{CH_2}	(Å)	3.93	3.93	3.93	3.905
ε_{CH_3}	(K)	114.0	98.1	104.0	88.1
ε_{CH_2}	(K)	47.0	47.0	47.0	59.4
K_r	($K/Å^2$)	96,500	96,500	96,500	96,500
b_{eq}	(Å)	1.54	1.54	1.54	1.54
K_θ	(K/rad^2)	62,500	62,500	62,500	62,500
θ_{eq}	(°)	114.0	114.0	114.0	112.0
V_0	(K)	0	0	0	0
V_1	(K)	355.04	355.04	355.04	355.03
V_2	(K)	−68.19	−68.19	−68.19	−68.19
V_3	(K)	701.32	701.32	701.32	791.32

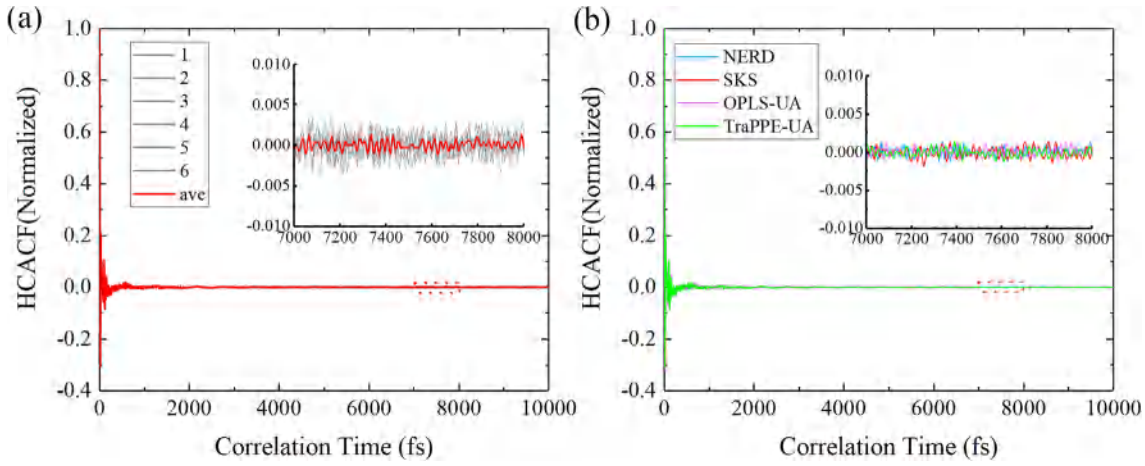

Fig. 2. (color online). The normalized HCACF: (a) Six independent runs of EMD simulations with the SKS model; (b) The averaged normalized HCACF with four different UA models.

between the MD simulation results and those of data from NIST are calculated as ARD $= \left|\lambda^{sim} - \lambda^{NIST}\right| / \lambda^{NIST} \times 100\%$, where λ^{sim} and λ^{NIST} denote the thermal conductivity values from MD simulation and the NIST data, respectively.

Thermal conductivities of *n*-decane are calculated via EMD simulations with different force field models at a pressure of 3 MPa. Since the typical temperature of RP-3 aviation kerosene in the cooling channel for scramjet applications is less than the critical temperature (Tc = 645.04 K), we choose the temperature range of 350–600 K in our MD simulations. Firstly, four all-atoms force field models, including the AMBER model, COMPASS model, L-OPLS model and OPLS-AA model, are compared with the TraPPE-UA model. The values of the computed thermal conductivities are compared to the corresponding NIST data [45], as shown in Fig. 5. For TraPPE-UA, AMBER, COMPASS, L-OPLS and OPLS-AA model, the averaged ARDs (AARDs) between the MD simulation results and NIST data are 5.01%, 119.26%, 137.72%, 153.02%, and 138.18%, respectively. It can be concluded that all-atom force field results are heavily overestimated and almost fails to predict thermal conductivities of the *n*-decane, while the TraPPE-UA model is able to accurately replicate the NIST results. Such a significant overestimation of the thermal conductivity for all-atom force field models also has been observed in earlier studies [39,46] for some of the alkanes. Zhang et al. [46] guessed that the better performance of UA model possibly could be explained by the remove of high-frequency degrees of freedom from the simulation, which

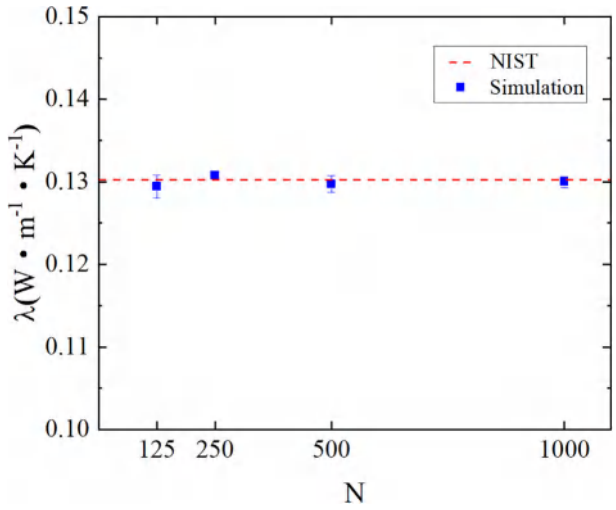

Fig. 4. (color online). Computed thermal conductivity of *n*-decane with different system sizes.

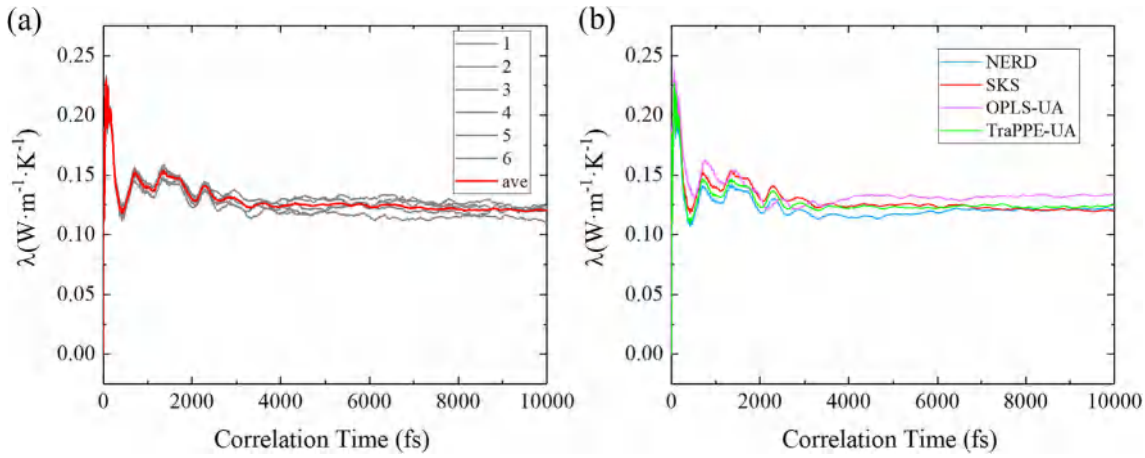

Fig. 3. (color online). Thermal conductivity calculated by numerical integration of the autocorrelation function. (a) The calculated thermal conductivity in six independent runs;(b) the averaged thermal conductivity with different UA models.

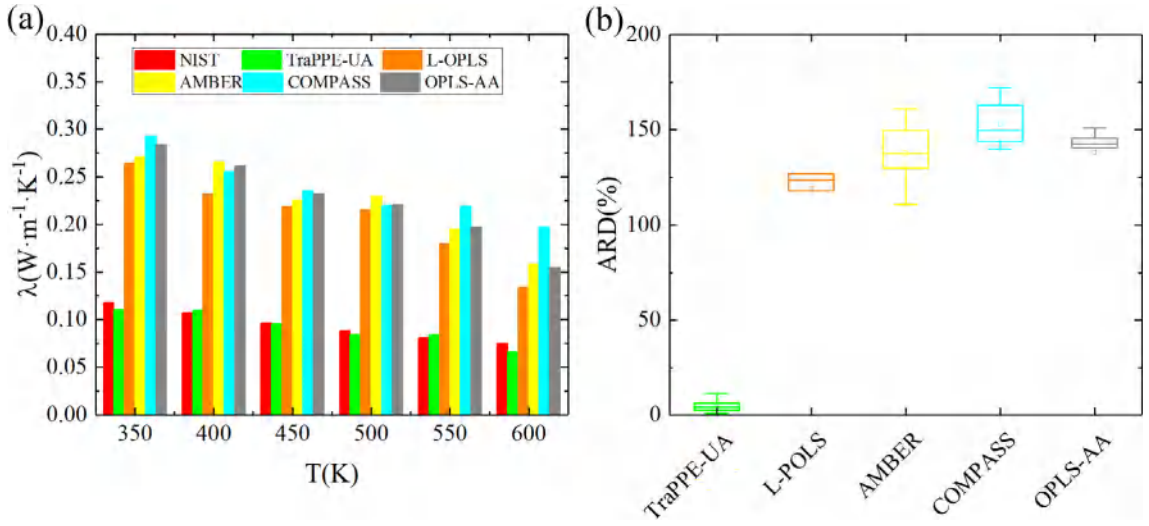

Fig. 5. (color online). Comparison of thermal conductivity calculated by EMD simulation with four all-atoms force field models and an UA model of TraPPE-UA.

act as quantum–mechanical oscillators in their ground state and do not contribute to thermal conduction. Nazarychev et al. [39] suggested that all-atom models overestimate the thermal conductivity in the highly disordered liquid state because of the shorter phonon free path and the lower scattering of phonons due to the significantly larger number of atoms in the all-atom systems compared to the UA model. However, these explanations may be not convincing. For example, it is questionable whether high-frequency degrees of freedom and the shorter phonon free path cause the overestimation of the thermal conductivity for all-atom force field models. The reasons for such an overestimation of the thermal conductivity of *n*-decane for all-atom force field models should be further explored.

We further compare the different UA models in the EMD simulations for the thermal conductivity of *n*-decane. Here four UA models, including SKS, TraPPE-UA, NERD and OPLS-UA, are adopted and compared. During these simulations, the temperature range is 298.87–512.46 K, and the pressure is 3 MPa. It should be noted that the temperatures are selected to be the same as those which have been used in Ref. [47] for RP-3 aviation kerosene. Thus, our results can be used in future investigations of alternative fuel model for RP-3 aviation kerosene. As seen from Fig. 6, the averaged absolute relative deviation (AARD) calculated by the four models is less than 10%. SKS model has the best overall performance, with an AARD value of 3.67%, indicating that SKS model is able to describe the thermal conductivity of *n*-decane more accurately.

3.2. Prediction results by RNEMD simulations

In the RNEMD simulations, we initially set up a simulation box containing 500 *n*-decane molecules. The total number of *n*-decane molecules in the system is same to that in our EMD simulations. The corresponding simulation box size is 3L × 3L × 20L(3L = 29 Å), as shown in Fig. 7. The simulation box is subdivided into 20 slabs (each with width of L) along the z coordinate. Slab 1 and slab 20 are defined as the cold slab and slab N/2 + 1 as the hot slab. Thermal energy is extracted at a constant rate from cold slab and added to hot slabs. First, the influence of the kinetic energy swap rate on the computed thermal conductivity is evaluated, Since the above section has shown that the SKS model has the best performance among the compared force field models in predicting the thermal conductivity of *n*-decane, the SKS model is selected for

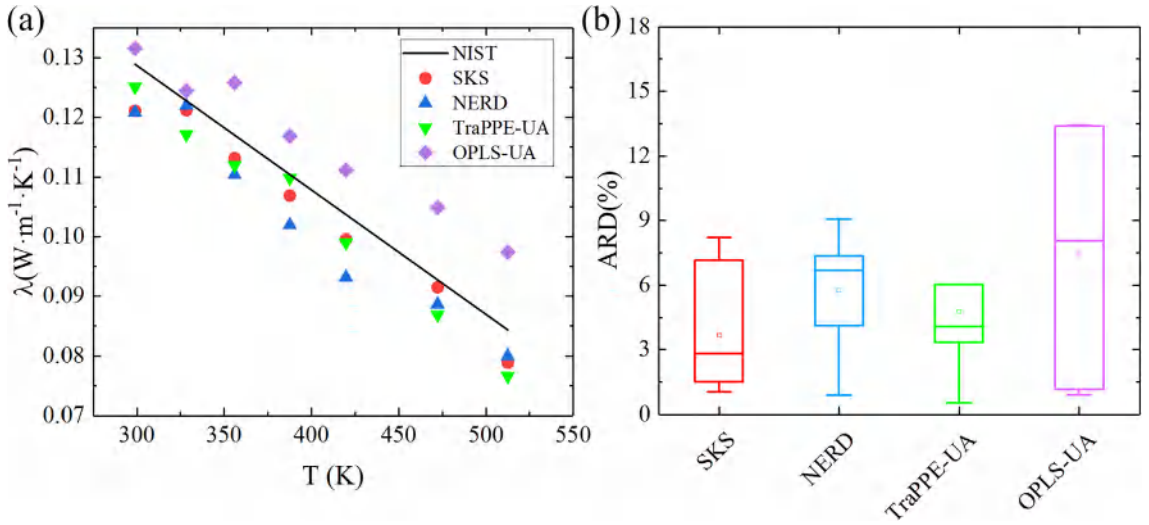

Fig. 6. (color online). EMD simulation results and deviations for four selected UA models.

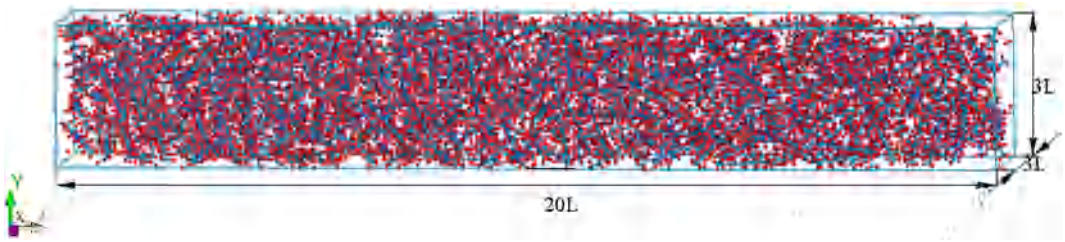

Fig. 7. (color online). Simulation system for the RNEMD simulation of thermal conductivity of *n*-decane.

the RNEMD simulations. Here the kinetic energy swap rate N_s means kinetic energy exchange is performed every N_s steps in the RNEMD simulations.

Fig. 8 shows the *n*-decane temperature profile with different swap rates between 500 and 10000 at 512.46 K. The corresponding temperature differences and the computed thermal conductivities are shown in Fig. 9. It can be observed that a swap rate N_s = 5000 is appropriate. In fact, overfrequency switching disturbances should be avoided, as they will lead to a larger temperature gradient in the simulation box. ΔT is too big and can lead to fluid in the coldest slab act like supercooled liquid, while slowing the movement of molecules in the slab. The resulting temperature profile computed at different given temperatures (N_s = 5000) for *n*-decane is plotted in Fig. 10.

Then four UA-force field models (SKS, TraPPE-UA, NERD&OPLS-UA) have been used during RNEMD simulations to predict the thermal conductivity of *n*-decane for the same previous molecular sitting and boundary conditions. The thermal conductivity of *n*-decane at supercritical pressure of 3 MPa is predicted by RNEMD method and compared with the reference value given by NIST as shown in Fig. 11. The thermal conductivities calculated by RNEMD with SKS model are compared with the NIST data. It can be seen that the predicted values by the SKS model are more consistent with the NIST data compared with other models, and the AARD of the SKS model is 6.0%.

3.3. Comparisons of EMD, RNEMD results, NIST data, and the RP-3 experimental data

To make a comprehensive comparison of the prediction performance for the thermal conductivity values of *n*-decane between

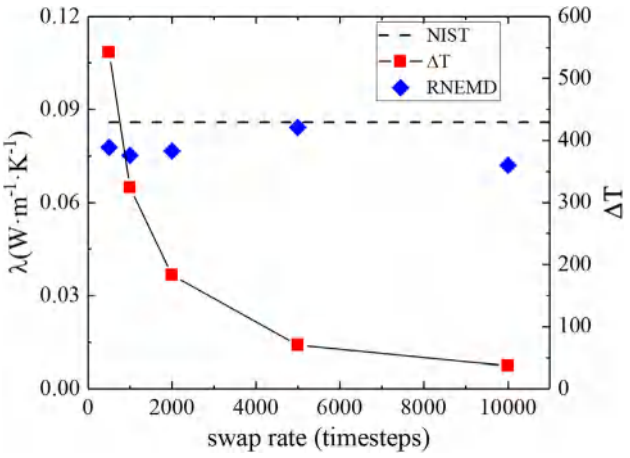

Fig. 9. (color online). *n*-Decane thermal conductivity of different swap rates at 512.46 K.

EMD and RNEMD method, a series of EMD and RNEMD simulations are conducted at pressures of 0.1 MPa and 5 MPa, respectively. The calculated thermal conductivity results are compared with NIST data as shown in Fig. 12 where the thermal conductivity of RP-3 at given pressures and temperatures are also provided. When compared with the NIST data, the AARDs from the EMD and RNEMD simulation results at pressure of 0.1 MPa are 1.52% and 3.16%, respectively; the AARDs of EMD and RNEMD simulation results at a pressure of 5 MPa are 4.76% and 11.09%, respectively. The corresponding simulations results at pressure of 3 MPa calculated

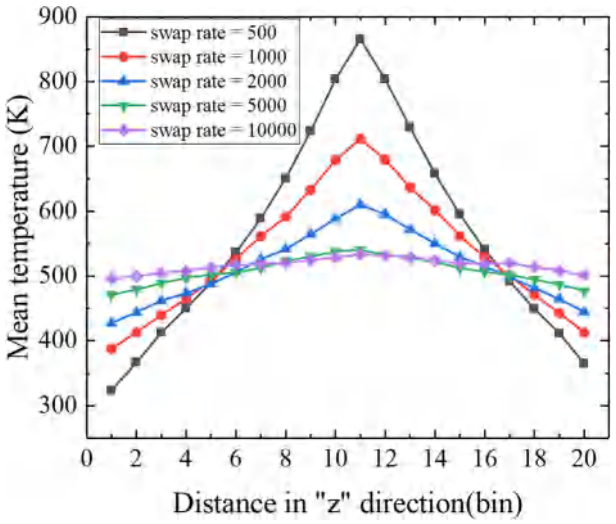

Fig. 8. (color online). *n*-Decane temperature profile of different swap rates at 512.46 K.

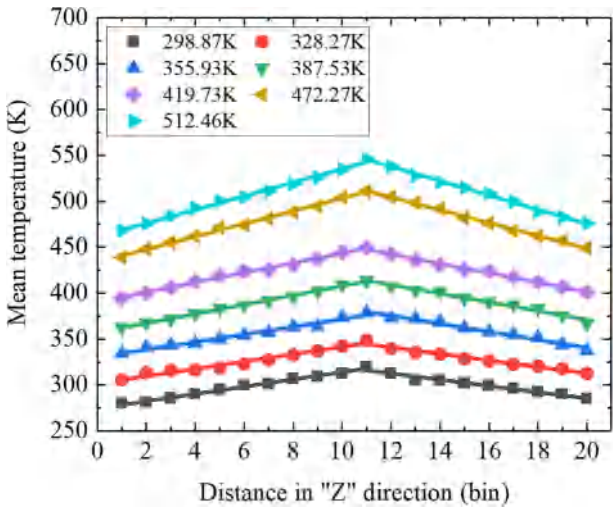

Fig. 10. (color online). Resulting temperature profile with kinetic energy swap rates equal to 5000 time steps for *n*-decane.

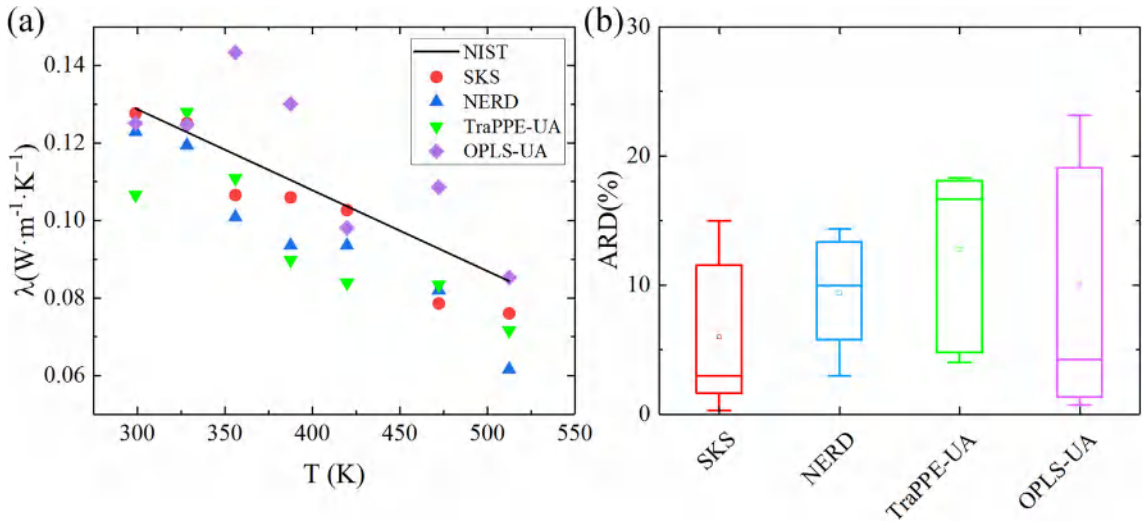

Fig. 11. (color online). Thermal conductivities calculated by RNEMD simulations and their deviations with different force field models. (a) Simulation results; (b) ARDs.

above are also provided in Fig. 12(b). It can be concluded that the EMD methods show better prediction accuracy than the RNEMD methods. Moreover, the EMD and RNEMD simulation results can also be compared with the experimental data of RP-3 aviation kerosene [47] for the MD study of one-component surrogate fuel for RP-3. When compared with the experimental data of RP-3 aviation kerosene, the AARDs of EMD and RNEMD simulation results at different pressures and temperatures are 2.05% and 6.34%, respectively.

3.4. Local structures

The particle radial distribution function (RDF) can reflect the local structure of the fluid, which is described as [48]:

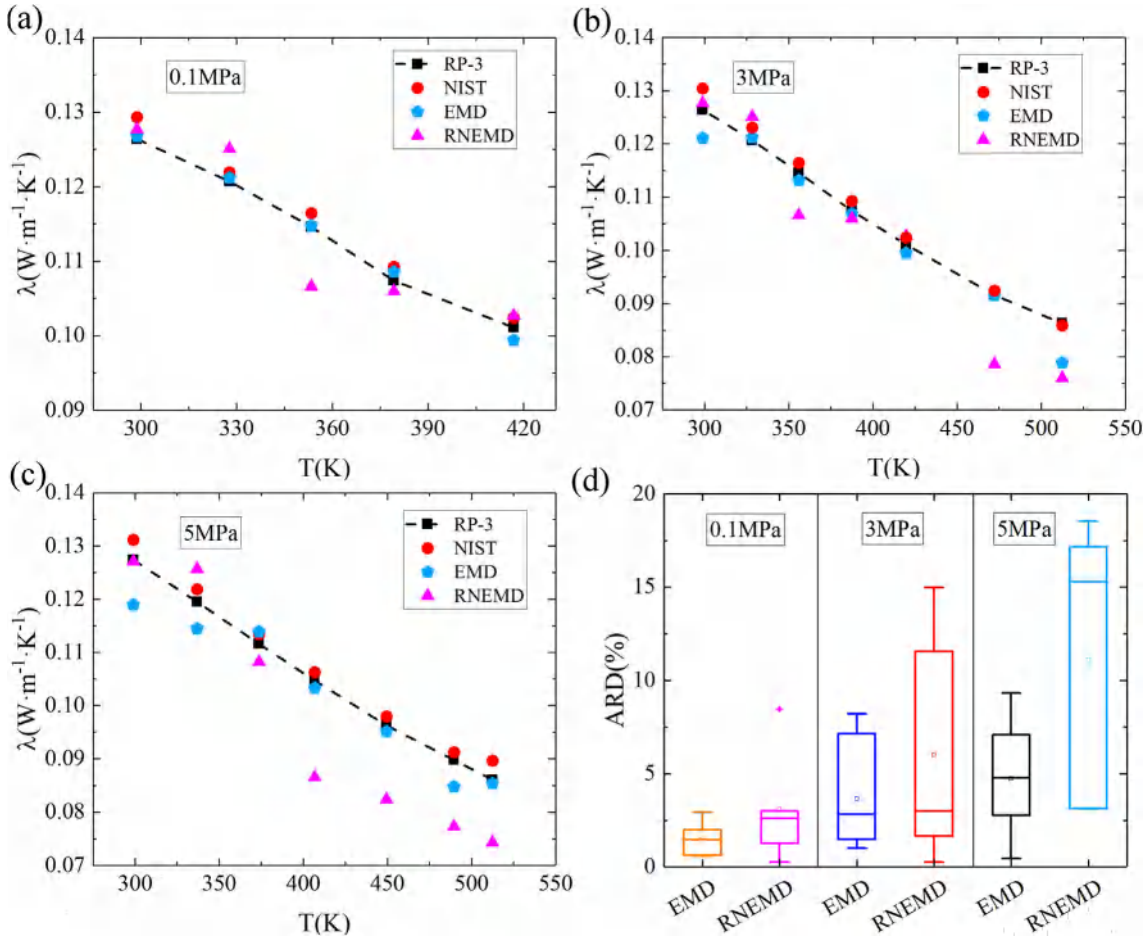

Fig. 12. (color online). EMD and RNEMD simulation results for *n*-decane compared with NIST data and experimental data of RP-3 at different pressures.

$$g_{\alpha\beta}(r) = \frac{1}{4\pi\rho_\beta r^2}\left[\frac{dN_{\alpha\beta}(r)}{dr}\right] \quad (9)$$

where ρ_β is the number density of species β and $N_{\alpha\beta}$ is the mean number of β-type particle lying in a sphere of radius r centered on a α-type particle.

Here the RDFs of *n*-decane molecules are calculated with the SKS force field at a pressure of 3 MPa and temperatures ranging from 298.87 to 512.46 K, as shown in Fig. 13. The RDFs of pseudoatoms CH_3-CH_3 and CH_2-CH_2 are calculated at different temperature and shown in Fig. 13(a).and 13(b), respectively. It can be observed that the magnitudes of the primary peaks of $g(r)_{CH_3-CH_3}$ and $g(r)_{CH_2-CH_2}$ are sensitive to the temperatures. With the increasing of temperature, the magnitudes of the primary peak decrease. This means that the higher the temperature, the higher the kinetic energy of the molecules, hence the smaller the aggregation. For $g(r)_{CH_3-CH_3}$, it can be observed apparently that the primary peaks are shifted from 4.15 Å to 4.5 Å when temperatures increase from 298.87 K to 512.46 K. With the increase of temperature, the thermal motion of molecules intensifies, and the system becomes loose and disorderly. Since the pseudoatoms CH_3 locate at the end of each *n*-decane molecules chain, the shift of the primary peaks of $g(r)_{CH_3-CH_3}$ indicates that the end to end distances of the *n*-decane molecules chains become larger with the increasing of the temperature, thus decreasing the thermal conductivity.

4. Conclusions

In this paper, EMD and RNEMD simulations are conducted and compared in the prediction of the thermal conductivity of *n*-decane at sub/supercritical pressure. Four different UA force field models and four all-atomic field models are assessed in the simulations. The main conclusions are derived as follows:

- The UA force field models exhibit much better performance than the all-atom force field models for the prediction of the thermal conductivity of the *n*-decane at sub/supercritical pressure..
- EMD methods show better prediction accuracy than the RNEMD methods with the same UA force field models.
- The SKS force field model has the best prediction accuracy among all force field models.
- The results by EMD simulations with SKS force field model are in good agreement with the referenced NIST data, and the overall AARD for the single component substitute of RP-3 aviation kerosene by *n*-decane is below 3%.

n-Decane is the most commonly used components in surrogate of RP-3 aviation kerosene for studying the thermophysical properties under subcritical and supercritical conditions in the regeneration cooling systems and the engine injection systems. In fact, a MD study directly on the surrogate multi-component blend of hydrocarbons is necessary, and may be more valuable. However, for the studies of the mixtures via MD simulations, the thermophysical properties of each components in the mixtures should be studied separately first to find the appropriate force field model and simulation strategies. The finding of this work could provide important guidance for the investigation of thermal conductivity of n-alkanes and n-alkane-based fuels.

CRediT authorship contribution statement

Xueming Yang: Conceptualization, Methodology, Validation, Writing – original draft. **Yue Gao:** Investigation, Writing – review & editing. **Mingli Zhang:** Visualization, Validation. **Wenchao Jiang:** Writing – review & editing, Validation. **Bingyang Cao:** Supervision, Software.

Declaration of Competing Interest

The authors declare that they have no known competing financial interests or personal relationships that could have appeared to influence the work reported in this paper.

Acknowledgments

This research is supported by the National Science and Technology Major Project of China (Grant No. 2017-III-0005-0030) and the Natural Science Foundation of Hebei Province of China (Grant No. E2019502138).

Appendix A. Supplementary material

Supplementary data to this article can be found online at https://doi.org/10.1016/j.molliq.2021.117478.

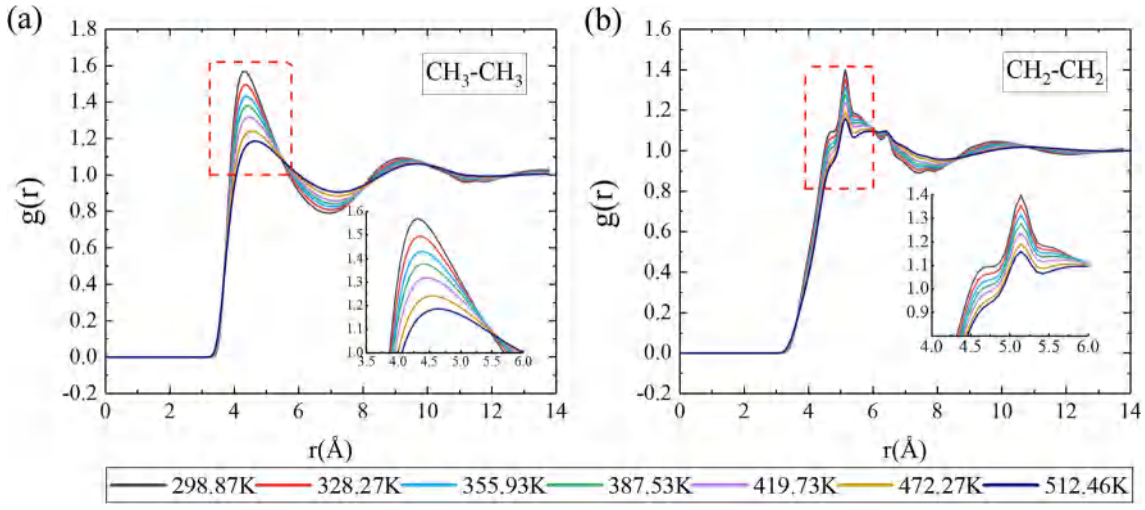

Fig. 13. (color online). RDF between different pseudoatoms types for *n*-decane: (a) CH_3-CH_3; (b) CH_2-CH_2.

References

[1] S. Maskey, B.H. Morrow, M.Z. Gustafson, D.J. Luning Prak, P.T. Mikulski, J.A. Harrison, Systematic examination of the links between composition and physical properties in surrogate fuel mixtures using molecular dynamics, Fuel 261 (2020) 116247, https://doi.org/10.1016/j.fuel.2019.116247.

[2] H. Pu, S. Li, S. Jiao, M. Dong, Y. Shang, Numerical investigation on convective heat transfer to aviation kerosene flowing in vertical tubes at supercritical pressures, Int. J. Heat Mass Transf. 118 (2018) 857–871, https://doi.org/10.1016/j.ijheatmasstransfer.2017.11.029.

[3] X. Li, S. Zhang, J. Qin, W. Bao, Parametric analysis on the thermal behavior of cracking hydrocarbon fuel flow inside asymmetry heated cooling channels with micro-ribs, Int. J. Heat Mass Transf. 160 (2020) 120154, https://doi.org/10.1016/j.ijheatmasstransfer.2020.120154.

[4] D. Sun, C. Li, Y. Du, L. Kou, J. Zhang, Y. Li, Z. Wang, J. Li, H. Feng, J. Lu, Effects of endothermic hydrocarbon fuel composition on the pyrolysis and anti-coking performance under supercritical conditions, Fuel 239 (2019) 659–666, https://doi.org/10.1016/j.fuel.2018.11.003.

[5] T. Edwards, L.Q. Maurice, Surrogate mixtures to represent complex aviation and rocket fuels, J. Propuls. Power. 17 (2) (2001) 461–466, https://doi.org/10.2514/2.5765.

[6] Y. Wang, P.-X. Jiang, Y. Zhu, A novel global reaction modeling approach considering the effects of pressure on pyrolysis of n-decane at supercritical pressures, Fuel 287 (2021) 119416, https://doi.org/10.1016/j.fuel.2020.119416.

[7] D.J. Luning Prak, J.M. Fries, R.T. Gober, P. Vozka, G. Kilaz, T.R. Johnson, S.L. Graft, P.C. Trulove, J.S. Cowart, V. Densities, Speeds of Sound, Bulk Moduli, Surface Tensions, and Flash Points of Quaternary Mixtures of n-Dodecane (1), n-Butylcyclohexane (2), n-Butylbenzene (3), and 2,2,4,4,6,8,8-Heptamethylnonane (4) at 0.1 MPa as Potential Surrogate Mixtur, J. Chem. Eng. Data. 64 (2019) 1725–1745, https://doi.org/10.1021/acs.jced.8b01233.

[8] A. Violi, S. Yan, E.G. Eddings, A.F. Sarofim, S. Granata, T. Faravelli, E. Ranzi, Experimental formulation and kinetic model for JP-8 surrogate mixtures, Combust. Sci. Technol. 174 (11-12) (2002) 399–417, https://doi.org/10.1080/00102200215080.

[9] P. Dagaut, On the kinetics of hydrocarbons oxidation from natural gas to kerosene and diesel fuel, Phys. Chem. Chem. Phys. 4 (2002) 2079–2094, https://doi.org/10.1039/b110787a.

[10] M.L. Huber, B.L. Smith, L.S. Ott, T.J. Bruno, Surrogate mixture model for the thermophysical properties of synthetic aviation fuel S-8: Explicit application of the advanced distillation curve, Energy Fuels 22 (2) (2008) 1104–1114, https://doi.org/10.1021/ef700562c.

[11] Y. Liu, Y. Yan, C. Dai, J. Li, A simplified chemical reaction mechanism for surrogate fuel of aviation kerosene, Chem. Res. Chinese Univ. 33 (2) (2017) 274–281, https://doi.org/10.1007/s40242-017-6280-1.

[12] Y. Yan, Y. Liu, W. Fang, Y. Liu, J. Li, A simplified chemical reaction mechanism for two-component RP-3 kerosene surrogate fuel and its verification, Fuel 227 (2018) 127–134, https://doi.org/10.1016/j.fuel.2018.04.092.

[13] J. Liu, E. Hu, W. Zeng, W. Zheng, A new surrogate fuel for emulating the physical and chemical properties of RP-3 kerosene, Fuel. 259 (2020) 116210, https://doi.org/10.1016/j.fuel.2019.116210.

[14] KeKe Xu, H. Meng, Analyses of surrogate models for calculating thermophysical properties of aviation kerosene RP-3 at supercritical pressures, Sci. China Technol. Sci. 58 (3) (2015) 510–518, https://doi.org/10.1007/s11431-014-5752-5.

[15] Y. Zhu, B.o. Liu, P. Jiang, Experimental and numerical investigations on n-decane thermal cracking at supercritical pressures in a vertical tube, Energy and Fuels. 28 (1) (2014) 466–474, https://doi.org/10.1021/ef401924s.

[16] X. Yang, M. Zhang, Y. Gao, J. Cui, B. Cao, Molecular dynamics study on viscosities of sub / supercritical n-decane, n-undecane and n-dodecane, J. Mol. Liq. 335 (2021) 116180, https://doi.org/10.1016/j.molliq.2021.116180.

[17] N.D. Kondratyuk, V.V. Pisarev, Predicting shear viscosity of 1,1-diphenylethane at high pressures by molecular dynamics methods, Fluid Phase Equilibria, https://doi.org/10.1016/j.fluid.2021.113100.

[18] A. Alkhwaji, S. Elbahloul, M.Z. Abdullah, K.F.B.A. Bakar, Selected water thermal properties from molecular dynamics for engineering purposes, J. Mol. Liq. 324 (2021) 114703, https://doi.org/10.1016/j.molliq.2020.114703.

[19] J. Nichele, A.B. de Oliveira, L.S.d.B. Alves, I. Borges, Accurate calculation of near-critical heat capacities CP and CV of argon using molecular dynamics, J. Mol. Liq. 237 (2017) 65–70.

[20] Z.B. Rózsa, B. Minofar, D. Řeha, B. Viskolcz, M. Szőri, From the vapor-liquid equilibrium to the supercritical condition. Molecular dynamics modeling of 1,3-butadiene, J. Mol. Liq. 315 (2020), https://doi.org/10.1016/j.molliq.2020.113702.

[21] K. Ogiwara, Y. Arai, S. Saito, Thermal conductivities of liquid hydrocarbons and their binary mixtures, Indust. Eng. Chem. Fund. 19 (3) (1980) 295–300, https://doi.org/10.1021/i160075a011.

[22] H. Kashiwagi, M. Oishi, Y. Tanaka, H. Kubota, T. Makita, Thermal conductivity of fourteen liquids in the temperature range 298–373K, International Journal of Thermophysics. 3 (2) (1982) 101–116, https://doi.org/10.1007/BF00503634.

[23] X. Zheng, D. Qu, F.a. Zhang, Y.u. Liu, G. Qin, Measurements and calculations of thermal conductivity for liquid n-octane and n-decane, Fluid Phase Equilibria. 533 (2021) 112940, https://doi.org/10.1016/j.fluid.2021.112940.

[24] T. Ohara, T. Chia Yuan, D. Torii, G. Kikugawa, N. Kosugi, Heat conduction in chain polymer liquids: Molecular dynamics study on the contributions of inter- and intramolecular energy transfer, J. Chem. Phys. 135 (3) (2011) 034507, https://doi.org/10.1063/1.3613648.

[25] J.I. Siepmann, S. Karaborni, B. Smit, Simulating the critical behaviour of complex fluids, Nature. 365 (6444) (1993) 330–332, https://doi.org/10.1038/365330a0.

[26] B. Smit, S. Karabomi, J. Ilja Siepmann, Computer simulations of vapor-liquid phase equilibria of n-alkanes, J. Chem. Phys. 102 (1995) 2126–2140, https://doi.org/10.1063/1.469563.

[27] M.G. Martin, J.I. Siepmann, Transferable potentials for phase equilibria. 1. United-atom description of n-alkanes, J. Phys. Chem. B. 102 (1998) 2569–2577, https://doi.org/10.1021/jp972543+.

[28] Shyamal K. Nath, Fernando A. Escobedo, Juan J. de Pablo, On the simulation of vapor-liquid equilibria for alkanes, J. Chem. Phys. 108 (23) (1998) 9905–9911, https://doi.org/10.1063/1.476429.

[29] William L. Jorgensen, Jeffry D. Madura, Carol J. Swenson, Optimized intermolecular potential functions for liquid hydrocarbons, J. Am. Chem. Soc. 106 (22) (1984) 6638–6646, https://doi.org/10.1021/ja00334a030.

[30] H. Sun, Compass: An ab initio force-field optimized for condensed-phase applications - Overview with details on alkane and benzene compounds, J. Phys. Chem. B 102 (1998) 7338–7364, https://doi.org/10.1021/jp980939v.

[31] William L. Jorgensen, David S. Maxwell, Julian Tirado-Rives, Development and testing of the OPLS all-atom force field on conformational energetics and properties of organic liquids, J. Am. Chem. Soc. 118 (45) (1996) 11225–11236, https://doi.org/10.1021/ja9621760.

[32] Eva Darian, Peter M. Gannett, Application of molecular dynamics simulations to spin-labeled oligonucleotides, J. Biomol. Struct. Dyn. 22 (5) (2005) 579–593, https://doi.org/10.1080/07391102.2005.10507028.

[33] Shirley W.I. Siu, Kristyna Pluhackova, Rainer A. Böckmann, Optimization of the OPLS-AA force field for long hydrocarbons, J. Chem. Theory Comput. 8 (4) (2012) 1459–1470, https://doi.org/10.1021/ct200908r.

[34] R. Kubo, M. Yokota, S. Nakajima, Statistical-mechanical theory of irreversible processes. Response to thermal disturbance, J. Phys. Soc. Japan. 12 (1957) 1203–1211, https://doi.org/10.1143/JPSJ.12.1203.

[35] Florian Müller-Plathe, A simple nonequilibrium molecular dynamics method for calculating the thermal conductivity, J. Chem. Phys. 106 (14) (1997) 6082–6085, https://doi.org/10.1063/1.473271.

[36] Steve Plimpton, Fast parallel algorithms for short-range molecular dynamics, Academic Press Professional 117 (1) (1995) 1–19.

[37] C. Chen, X. Jiang, Transport property prediction and inhomogeneity analysis of supercritical n-Dodecane by molecular dynamics simulation, Fuel. 244 (2019) 48–60, https://doi.org/10.1016/j.fuel.2019.01.181.

[38] R.W. Hockney, J.W. Eastwood, Computer Simulation Using Particles, Adam Hilger, NY, 1989.

[39] Victor M. Nazarychev, Artyom D. Glova, Igor V. Volgin, Sergey V. Larin, Alexey V. Lyulin, Sergey V. Lyulin, Andrey A. Gurtovenko, Evaluation of thermal conductivity of organic phase-change materials from equilibrium and non-equilibrium computer simulations: Paraffin as a test case, Int. J. Heat Mass Transf. 165 (2021) 120639, https://doi.org/10.1016/j.ijheatmasstransfer.2020.120639.

[40] X. Yang, X. Wang, W. Wang, Y. Fu, Q. Xie, Atomic-scale insights into interface thermal resistance between epoxy and boron nitride in nanocomposites, Int. J. Heat Mass Transf. 159 (2020) 1–8, https://doi.org/10.1016/j.ijheatmasstransfer.2020.120105.

[41] X. Yang, C. Duan, J. Xu, Y. Liu, B. Cao, A numerical study on the thermal conductivity of H2O/CO2/H2 mixtures in supercritical regions of water for coal supercritical water gasification system, Int. J. Heat Mass Transf. 135 (2019) 413–424, https://doi.org/10.1016/j.ijheatmasstransfer.2019.01.146.

[42] Xueming Yang, Yiyu Feng, Jiangxin Xu, Jianghao Jin, Yuanbin Liu, Bingyang Cao, Numerical study on transport properties of the working mixtures for coal supercritical water gasification based power generation systems, Appl. Therm. Eng. 162 (2019) 114228, https://doi.org/10.1016/j.applthermaleng.2019.114228.

[43] H. Guo, N. Zhao, Interfacial layer simulation and effect on Cu-Ar nanofluids thermal conductivity using molecular dynamics method, J. Mol. Liq. 259 (2018) 40–47, https://doi.org/10.1016/j.molliq.2018.03.001.

[44] Rajesh Khare, Juan de Pablo, Arun Yethiraj, Molecular simulation and continuum mechanics study of simple fluids in non-isothermal planar couette flows, J. Chem. Phys. 107 (7) (1997) 2589–2596, https://doi.org/10.1063/1.474570.

[45] E.W. Lemmon, M.L. Huber, M.O. McLinden, NIST Standard Reference Database 23: Reference Fluid Thermodynamic and Transport Properties-REFPROP, Version 9.1, National Institute of Standards and Technology, Standard Reference Data Program, Gaithersburg, 2013.

[46] Meimei Zhang, Enrico Lussetti, Luís E.S. de Souza, Florian Müller-Plathe, Thermal conductivities of molecular liquids by reverse nonequilibrium molecular dynamics, J. Phys. Chem. B. 109 (31) (2005) 15060–15067, https://doi.org/10.1021/jp0512255.

[47] G.Q. Xu, Z.X. Jia, J. Wen, H.W. Deng, Y.C. Fu, Thermal-Conductivity Measurements of Aviation Kerosene RP-3 from (285 to 513) K at Sub- and Supercritical Pressures, Int. J. Thermophys. 36 (4) (2015) 620–632, https://doi.org/10.1007/s10765-015-1840-4.

[48] Enrico Matteoli, G. Ali Mansoori, A simple expression for radial distribution functions of pure fluids and mixtures, J. Chem. Phys. 103 (11) (1995) 4672–4677, https://doi.org/10.1063/1.470654.